Annual Project Summary

High-resolution 3-D velocity model for Northridge-Los Angeles basin area from tomographic inversion of local arrival time data

External Grant Award Number: 03HQGR0064

Jose Pujol
Center for Earthquake Research and Information
The University of Memphis, Memphis, TN 38152
Phone: (901) 678-4827 Fax: (901) 678-4734 Email: pujol@ceri.memphis.edu

Non-technical summary

We determined a high-resolution 3-D P wave velocity model for an 80 km $\times$ 80 km area around the San Fernando valley using events recorded between 1980 and 2000 as well as aftershocks of the 1971 San Fernando earthquake recorded by a portable network. The total number of events and stations used were 13455 and 100. Most of the events are aftershocks of the 1994 Northridge earthquake. Our model shows an overall good agreement with the Southern California Earthquake Center (SCEC) model, but our model images the deep structure of the San Fernando valley better. A narrow and well-defined 10 km wide lineation of Northridge aftershocks occurred in the basement between about 10 and 20 km and define the fault that slipped during the mainshock. This fault plane inferred from the seismicity is in good qualitative agreement with the geodetic fault plane determined by Hudnut et al. (1996) assuming uniform slip. Horizontal velocity slices show that the Northridge earthquake occurred within a narrow basement wedge, which may have controlled the size of the earthquake. Comparison of our velocity model with a roughly N-S 50 km long density model derived by Langenheim et al. (2000) from the analysis of gravity data shows a surprisingly good agreement. Most of the aftershocks of the Northridge earthquake occurred within the basin, with a large concentration of them to the east of the eastern boundary of the mainshock fault plane. The latter events also dip to the southwest, most of them are shallower than about 14 km and form a band of seismicity within and near the edge of the basin. These events are not on the mainshock fault plane, and because the San Fernando aftershocks are also to the east of the Northridge fault plane, the San Fernando and the Northridge mainshocks occurred on en-echelon conjugate faults. In other words, the San Fernando fault did not truncate the Northridge fault, as commonly stated. On the other hand, an 8 km wide cross section along the density model referred to above shows that the Northridge aftershocks east of the mainshock and most of the aftershocks of the San Fernando earthquake occurred around a high-velocity basement block. We interpret this result as an indication that this basement high remained elevated during the opening of the basin, with the observed seismicity occurring in the weaker sedimentary rocks around its flanks.

Results

Although our research targeted a larger area, we concentrated on an area of 80 km $\times$ 80 km roughly centered at the San Fernando valley because of the large amount of data available and the relatively high station coverage. Our analysis proceeded in two stages. In the first one we used P wave arrival times from aftershocks of the Northridge earthquake recorded in 1994, while in the second stage data recorded between 1980 and 2000 were used. In both cases aftershock data from the San Fernando earthquake recorded by a portable network were included.

The iterative tomographic velocity inversion and earthquake relocation package of Benz (Benz et al., 1996) was used. This package includes software for the computation of travel times designed to handle sharp velocity discontinuities without approximations (Podvin and Lecomte, 1991), and the high resolution of our results derives from the use of this software.

The velocity model was parameterized in terms of $2 \times 2 \times 2$ km blocks. In the first stage we used 4177 events in the Northridge mainshock-aftershock sequence recorded by 63 permanent and portable stations and 799 events from the San Fernando aftershock sequence recorded by a network of 20 portable stations. To assess the effect of the initial velocity model in the inversion results two models were used. One was a coarse 3-D velocity model determined using the same inversion software applied to a 300 km $\times$ 300 km area with $5 \times 5 \times 3$ km blocks (Shen, 1999). The second model was the 3-D SCEC model (Magistrale et al., 2000). The results for the two models are different in the details only; the main features are similar. This shows that the dependence of the inversion model on the initial velocity model is relatively minor. Moreover, the inversion of realistic synthetic arrival times shows that our results are reliable.

In the second stage we inverted P wave arrival times from the San Fernando events and from 12656 events recorded between 1980 and 2000) (Fig. 1). The total number of seismic stations was 100. Although the number of events recorded during 1980-2000 is much larger, a number of quality criteria reduced the number of usable events. The number of iterations was ten and in the last iteration about 800 events were not used because they either did not satisfy additional quality criteria or had negative depths. The initial velocity model is the standard 1-D model based on the results of Hadley and Kanamori (1977). The upper layer in the 1-D model has a velocity of 5.5 km/s, which means that the sedimentary cover is not included. Our main results can be summarized as follows.

The most distinctive feature of our velocity model is its high resolution, which far exceeds that of other models (Pujol, 1996; Hauksson and Haase, 1997; Mori et al. 1995). and although the analysis of synthetic data showed that the velocity models obtained are not an artifact of the inversion technique, we looked for supporting evidence from other sources. The most obvious comparison is with the SCEC 3-D velocity model for the portion of that model with information derived from non-earthquake data. Figures 2 and 3 show the upper layer of our inversion model and the SCEC model. The overall agreement between the two models is good. The inversion model clearly shows part of the Los Angeles basin and the San Fernando Valley, as well as the Santa Monica and San Gabriel mountains. However, there is a conspicuous difference near the northern end of the line labeled **a**. Langenheim et al. (2000) derived a density model along this line based on the fitting of theoretical gravity data to observed data. The comparison of their model and the inversion velocities is surprisingly good (Fig. 4). In addition to the features referred to above, the velocity model also shows the presence of the Soledad basin, which is a relatively small feature. To appreciate the resolving power of the software and data we used, the initial velocity model is shown in Fig. 5. On the other hand, the SCEC model (Fig. 6) does not fit the density model as well as the inversion model and the surface expressions of the Santa Monica and San Gabriel mountains are not imaged. In addition, the depth of the low-velocity sediments in the San Fernando valley appears excessive. A further comparison between the inversion and SCEC models is provided by Figs. 7 and 8, which shows an overall good agreement, although the inversion model images the deep structure of the San Fernando valley better. According to Lutter et al. (2004) the basement velocity where the LARSE II transect crosses basement outcrop (beneath the weathered layers) in the Santa Monica Mountains and central Transverse Ranges is between 5.75 and 6.0 km/s and between 5.5 and 6.0 km/s, respectively. In the velocity cross sections shown here the 6 km/s contour line coincides with the boundary between the yellow and redish areas and will be used as the basin boundary.

Fig. 7 shows that most of the Northridge earthquake aftershocks occurred within the basin, with the basement activity concentrated in cross sections D and E along clear lineations that define the fault that slipped during the mainshock. This lineations are even narrower in Fig. 9, which shows the events that occurred in 1994 only. This fault plane inferred from the seismicity is in good qualitative agreement with the geodetic fault plane determined by Hudnut et al. (1996) assuming uniform slip. In addition, horizontal velocity slices show that the Northridge earthquake occurred within a narrow basement wedge (Fig. 10), which may have controlled the size of the earthquake.

A strong cluster of aftershocks in cross section D in Fig. 7 at about 10 km depth roughly along the fault plane may be associated with the fact that this is the area where the main shock intersected the bottom of the basin. The same conclusion was reached by Langenheim et al. (2000) from the analysis of gravity data. The events in cross section C in Fig. 9 between about 10 and 15 km depth around a distance of 20 km are likely to correspond to the Santa Susana fault. The corresponding events in Fig. 7 show a more diffuse zone of aftershocks.

The large concentration of aftershocks to the east of the green line in Fig. 1 did not occur on the mainshock fault plane. The events also dip to the southwest, most of them are shallower than about 14 km and form a band of seismicity within and near the edge of the San Fernando basin. Interestingly, the location of the largest Northridge aftershock, which occurred one minute after the mainshock, is in the vicinity of these events. Note that most of the San Fernando events also occurred to the east of the green line, which means that the San Fernando and the Northridge mainshocks occurred on en-echelon conjugate faults, so that the San Fernando fault did not truncate the Northridge fault, as commonly stated. On the other hand, Fig. 11 shows that these Northridge aftershocks and the aftershocks of the San Fernando earthquake occurred around a high-velocity basement block. We interpret this result as an indication that this basement high remained elevated during the opening of the basin, with the observed seismicity occurring in the weaker sedimentary rocks around its flanks.

Recently, Hauksson et al. (2003) and Shearer et al. (2003) produced catalogs of southern California aftershocks, and for comparison purposes their locations for the events in Fig. 1 are shown in Figs. 12-13 and 14-15. The two sets of locations are clearly different. The Hauksson et al. (2003) locations are some what more scattered than the locations shown in Figs. 1 and 7. The Shearer et al. (2003) locations are much more clustered, are somewhat to the east of the locations in Fig. 1, and are consistently deeper that those in Fig. 7. On average, the depth difference is 2.4 km.

Data availability

The velocity model and event locations are in binary and ASCII formats, respectively, and are available from J. Pujol (phone: 901-678-4827; email: pujol@ceri.memphis.edu).

References

Benz, H., B. Chouet, P. Dawson, J. Lahr, R. Page, and J. Hole (1996). Three-dimensional P and S wave velocity structure of Redoubt volcano, Alaska, *J. Geophys. Res.* **101**, 8111-8128.

Hadley, D. and H. Kanamori (1977). Seismic structures of the Transverse Ranges, California, *Geol. Soc. America Bull.* **88**, 1469-1478.

Hauksson E., and J. Haase (1997). Three dimensional Vp and Vp/Vs velocity models of the Los Angeles basin and central Transverse Ranges, California, *J. Geophys. Res.* **102**, 5423-5453.

Hauksson E., W-C. Chi, and P. Shearer (2003). Comprehensive waveform cross-correlation of southern California seismograms: Part 1. Refined hypocenters obtained using the double-difference method and tectonic implications (abstract), *Eos Trans. AGU* **84**(46), Fall Meet. Suppl., Abstract S21D-0325.

Hudnut, K., and ten others (1996). Co-seismic displacements of the 1994 Northridge, California, earthquake, *Bull. Seism. Soc. Am.* **86**, S19-S36.

Langenheim, V., A. Griscom, R. Jachens, and T. Hildenbrand (2000). Preliminary potential-field constraints on the geometry of the San Fernando basin, southern California, *U.S.G.S. Open-file Report* **00-219**.

Lutter, W. and 15 others (2004).Upper crustal structure from the Santa Monica mountains to the Sierra Nevada, southern California: tomographic results from the Los Angeles Regional Seismic Experiment, Phase II (LARSE II), *Bull. Seism. Soc. Am.* **94**, 619-632

Magistrale, H., S. Day, R. Clayton, and R. Graves (2000). The SCEC southern California reference three-dimensional seismic velocity model version 2, *Bull. Seism. Soc. Am.* **90**, S65-S76.

Mori, J., D. Wald, and R. Wesson (1995). Overlapping fault planes of the 1971 San Fernando and 1994, California earthquakes, *Geophys. Res. Lett.* **22**, 1033-1036.

Podvin, P., and I. Lecomte (1991). Finite difference computation of traveltimes in very contrasted velocity models: A massively parallel approach and its associated tools, *Geophys. J. Int.* **105**, 271-284.

Pujol, J. (1996), An integrated 3D velocity inversion – joint hypocentral determination relocation analysis of events in the Northridge area, *Bull. Seism. Soc. Am.* **86**, S138-155.

Shearer, P., E. Hauksson, G. Lin and D. Kilb (2003). Comprehensive waveform cross-correlation of southern California seismograms: Part 2. Event locations obtained using cluster analysis *Eos Trans. AGU* **84**(46), Fall Meet. Suppl., Abstract S21D-0326.

Shen, P. (1999). Simultaneous travel time inversion for 3D velocity model and earthquake locations: application to the Northridge, California, 1994 mainshock-aftershock sequence, M.S. thesis, The University of Memphis.

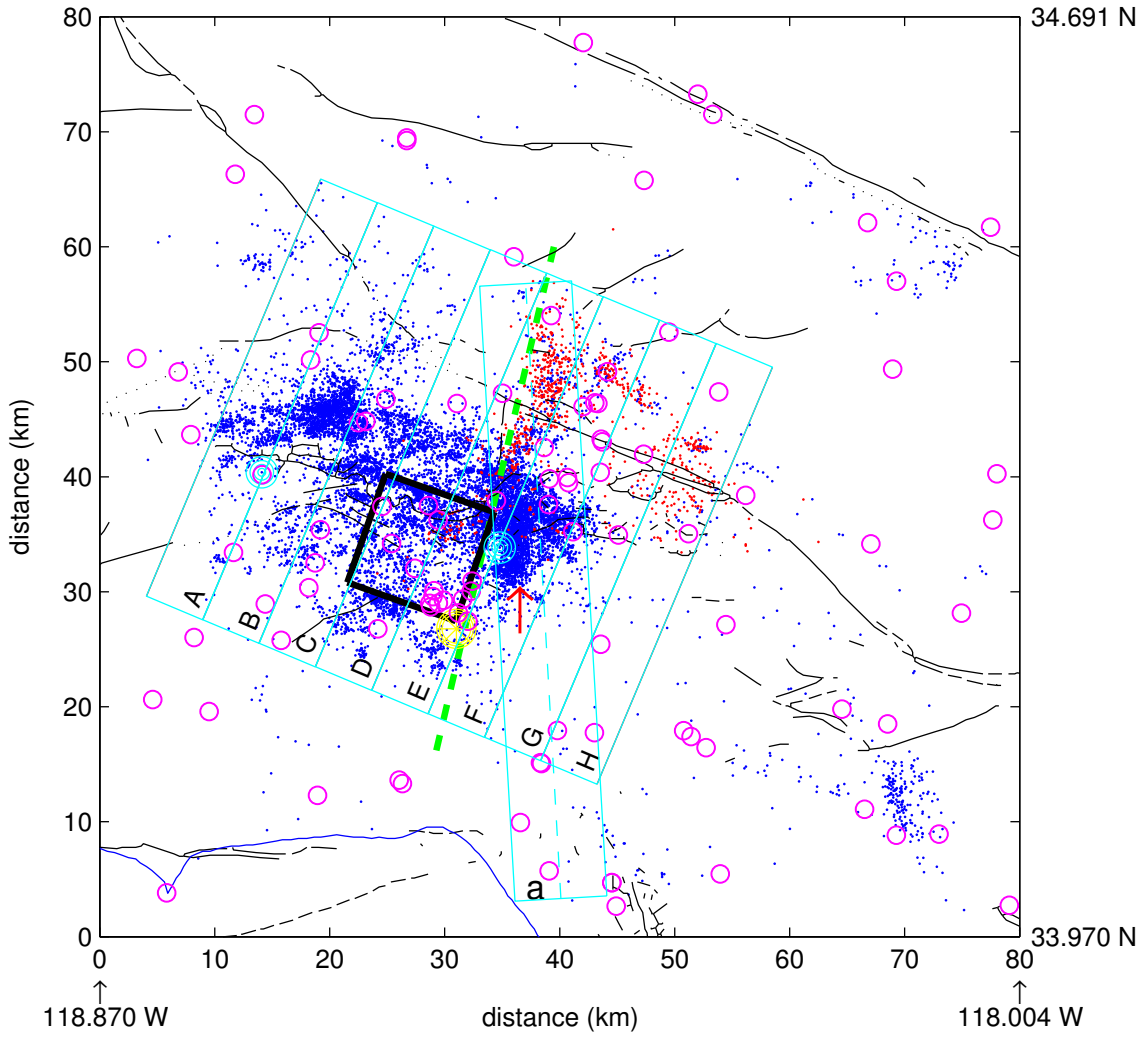

Figure 1: Area for which a 3-D velocity model has been determined. Blue dots indicate seismic events recorded between 1980 and 2000. Most of the events within the blue boxes are aftershocks of the Northridge earthquake. The red dots indicate aftershocks of the San Fernando earthquake recorded during February-April 1971 by a network of 20 portable stations. Red circles indicate seismic stations. The large yellow and two blue symbols indicate the Northridge mainshock and its largest aftershocks, which occurred one minute (M = 5.9, Box E) and about 11 hours (M = 5.6; Box A) later. All the event locations except those of the two largest aftershocks were determined as part of the velocity inversion - earthquake location process. The location of the M = 5.9 event is not well constrained. The bold rectangle is the projection of the fault plane determined by Hudnut et al. (1996) assuming uniform slip. The events in the boxes A through H and in box **a** are shown in cross section form in Figs. 7 and 11. Most of the San Fernando events are to the east of the green dashed line while the Northridge main shock rupture occurred to the west of that line. The prominent band of Northridge seismicity in a roughly N-S direction (identified by the arrow in box F) did not occur within the area that ruptured during the main shock.

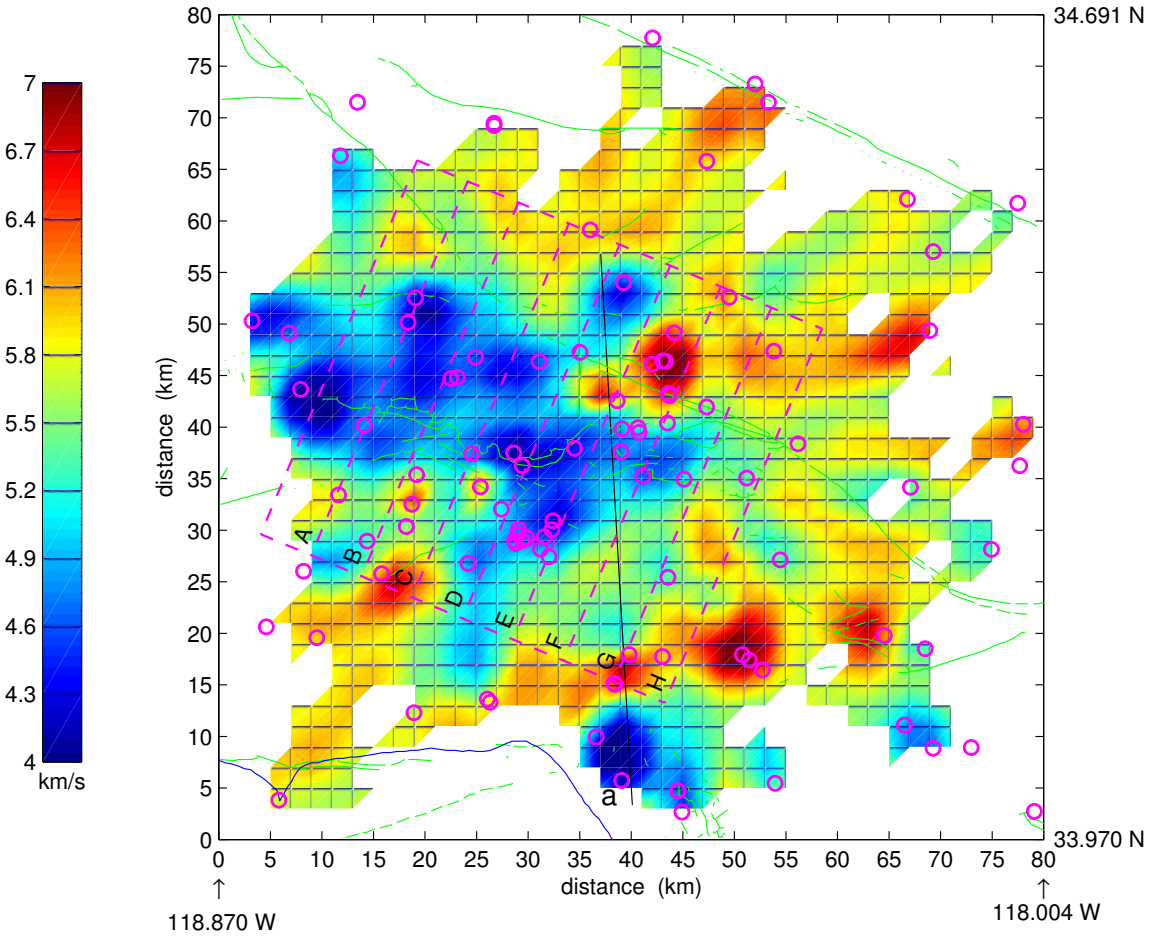

Figure 2: Map view of the upper layer of the 3-D velocity model determined by tomographic inversion. The ragged appearance is due to the fact that only blocks covered by more than five rays are shown. The initial velocity model was the layered model shown in Fig. 5. The central and southern low-velocity areas correspond to the San Fernando and Ventura basins and to the Los Angeles basin, respectively. The labeled boxes coincide with those in Fig. 1. Velocity cross sections are shown in Figs. 4 and 7.

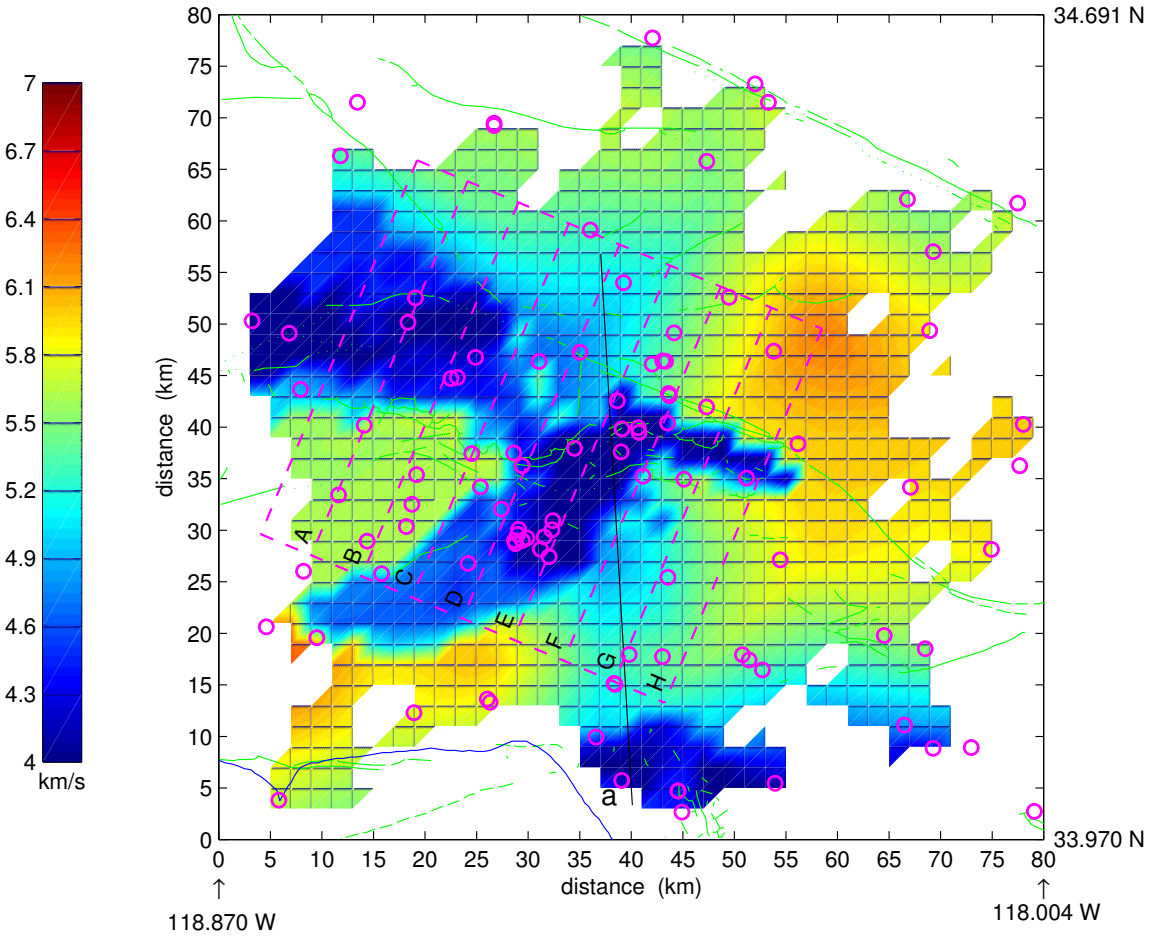

Figure 3: Similar to Fig. 2 for the SCEC 3-D velocity model (see Magistrale et al., 2000). Velocity cross sections are shown in Figs. 6 and 8.

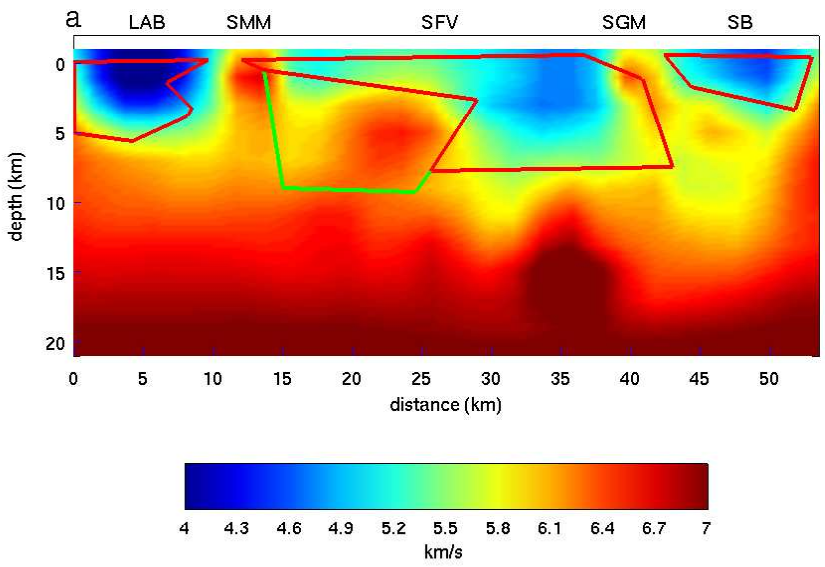

Figure 4: Velocity depth cross section along the dashed line in box **a** of Fig. 1 for the inversion model. All the blocks of the inversion model, regardless of the ray coverage are shown. The polygons represent the bodies (simplified) used by Langenheim et al. (2000) to match observed gravity profiles. The red lines bound materials with densities ranging between 2.00 and 2.55 g/cm^3. The area bounded by red and green lines corresponds to low-density basement (2.65 g/cm^3). Elsewhere in the figure the density is 2.71 g/cm^3. Note the excellent agreement between the extent of the low velocities in the Los Angeles (LAB), San Fernando (SFV) and Soledad (SB) basins and the low-density bodies in the Langenheim et al. (2000) model, as well the fact that that the surface expressions of the Santa Monica Mountains (SMM) and the San Gabriel Mountains (SGM) are correctly imaged by the velocity model.

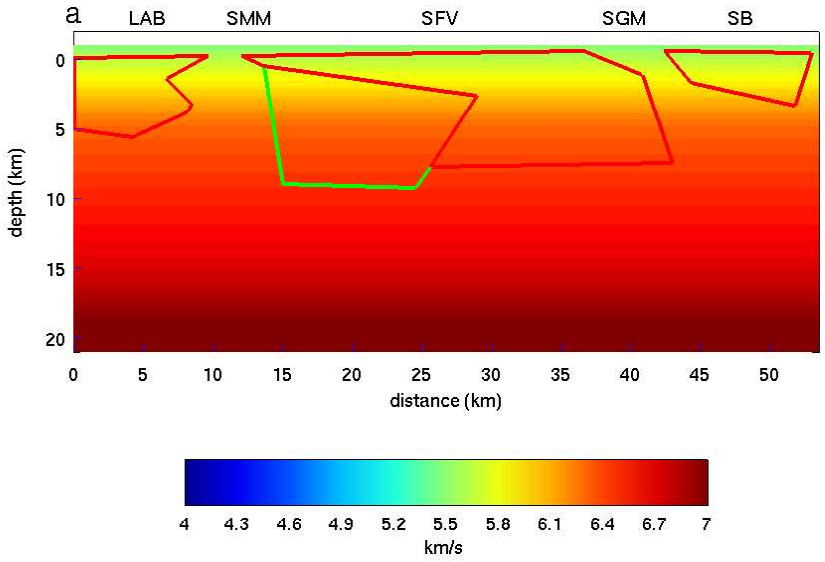

Figure 5: Similar to Fig. 4 for the initial velocity model.

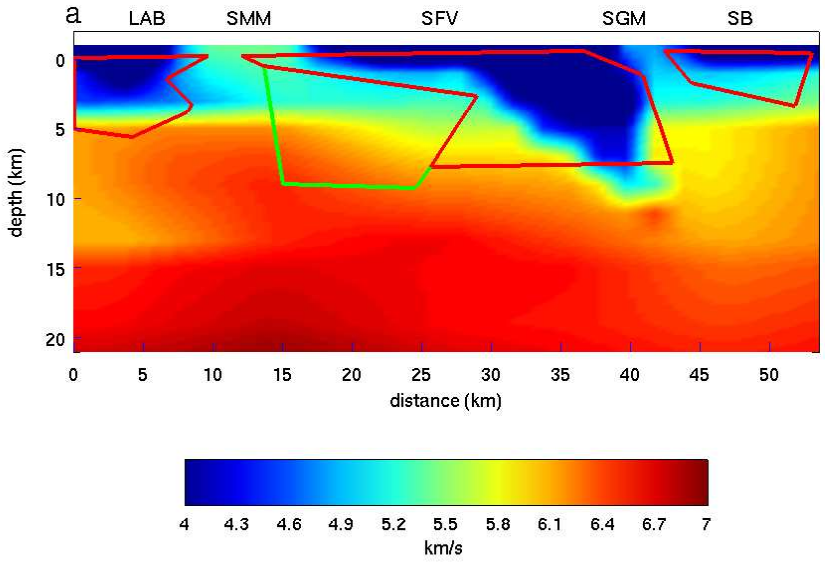

Figure 6: Similar to Fig. 4 for the SCEC 3-D velocity model. Note that this model does not fit the density model as well as the inversion model and that the surface expressions of the Santa Monica and San Gabriel mountains are not imaged. In addition, the depth of the low-velocity sediments in the San Fernando valley appears excessive.

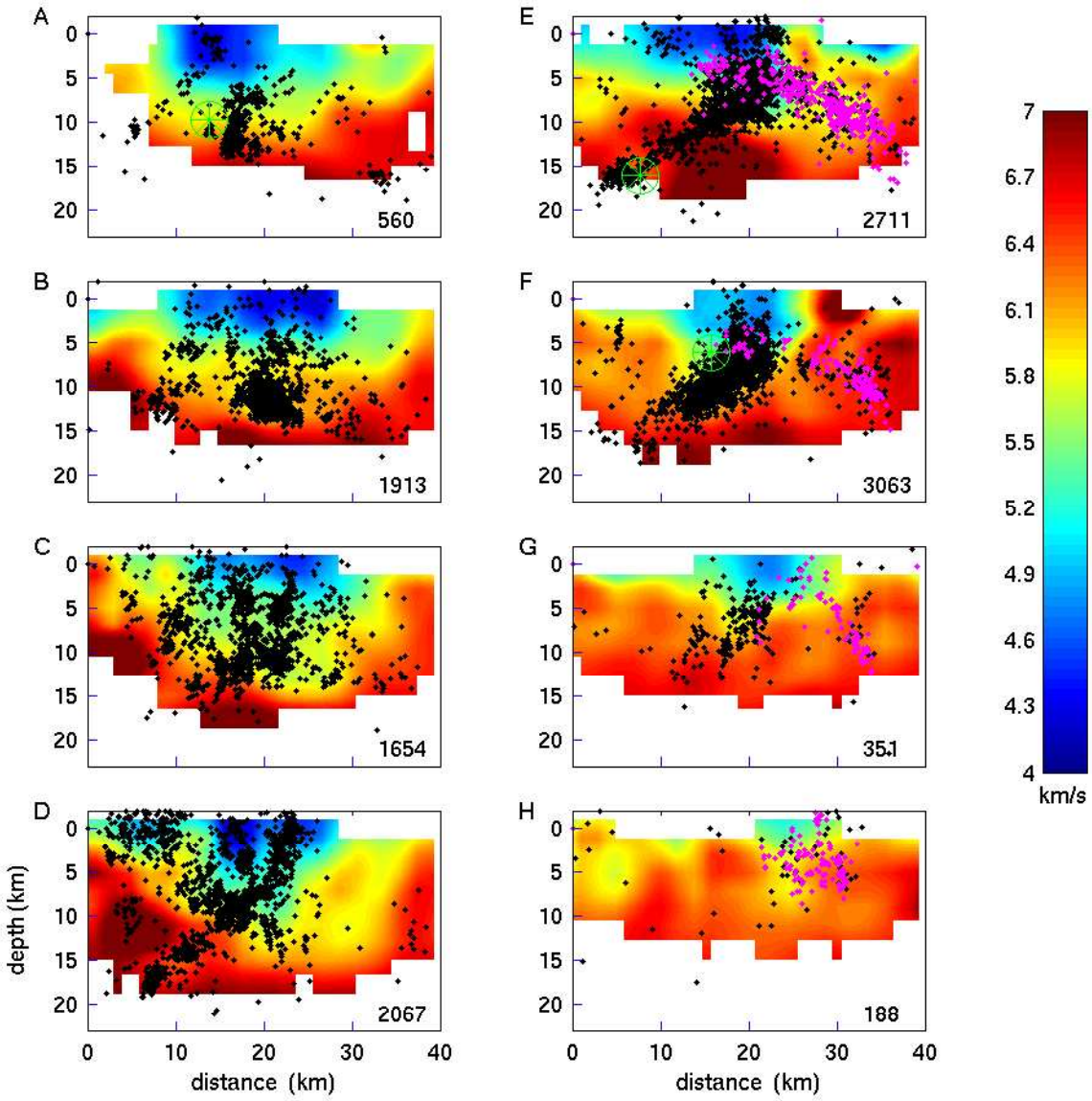

Figure 7: Depth cross sections for the velocity model and the events in the boxes A through H in Fig. 1. The width of the cross sections is 5.3 km. The letters are on the southern ends of the cross sections. Black and red dots indicate Northridge and San Fernando aftershocks. The large green symbols in cross sections E, A and F indicate the Northridge mainshock (18 km depth) and its two largest aftershocks (see Fig. 1). The number in the right lower corner of each cross section denotes the number of events. Only the velocity blocks covered by at least five rays are shown. Note the correlation between seismicity and velocity. The events between about 10 and 20 km in D and E are within high-velocity, basement rocks, and form narrow and well-defined lineations. These events span about 10 km horizontally and basically define the width of the fault that slipped during the main shock. The Northridge aftershocks in F correspond mostly to those indicated by an arrow in Fig. 1. Most of these events are shallower than about 14 km and form a band of seismicity within and near the edge of the basin. Most of the seismicity in A, B, and C occurs within the basin.

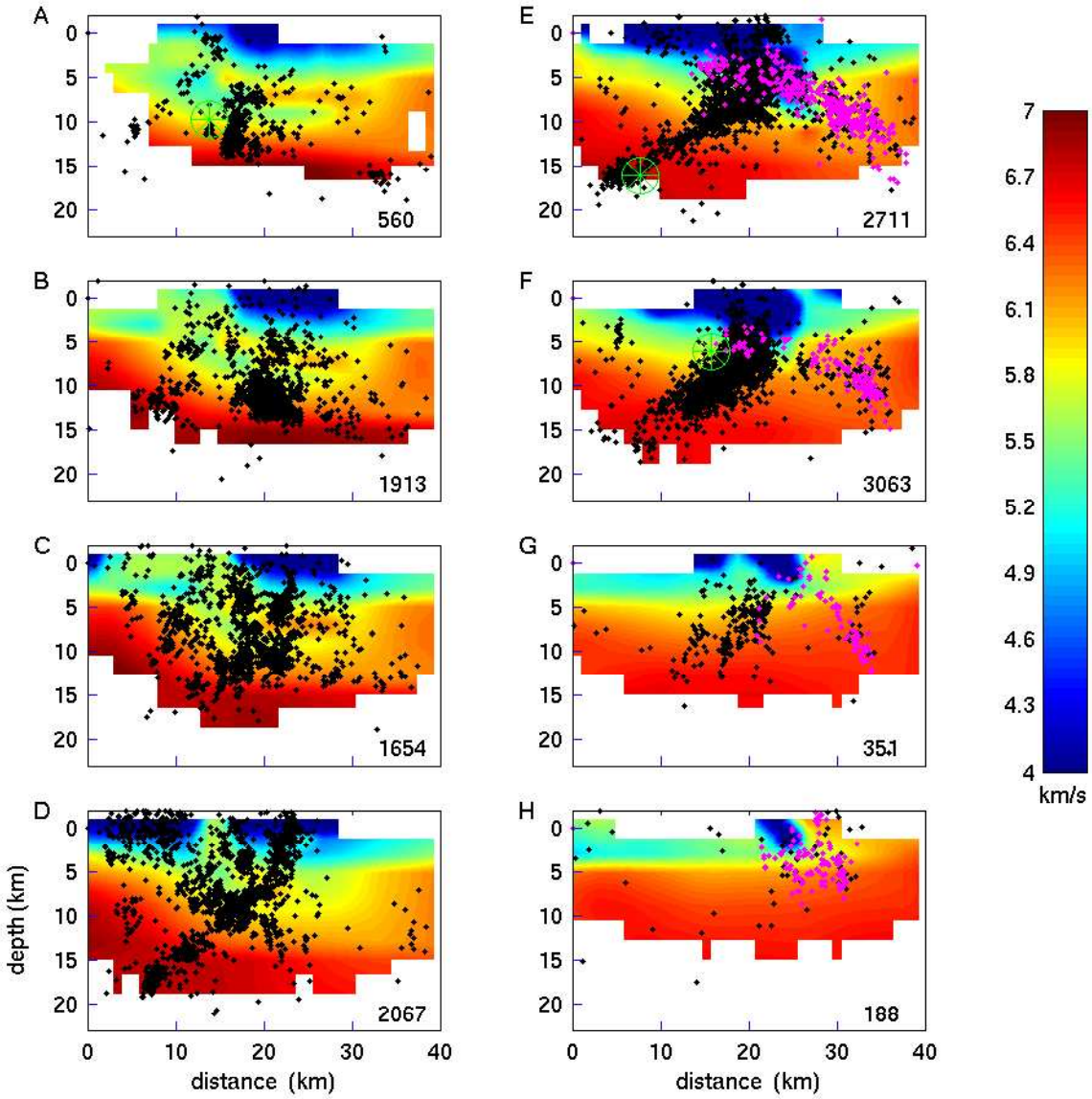

Figure 8: Similar to Fig. 7 for the SCEC 3-D velocity model.

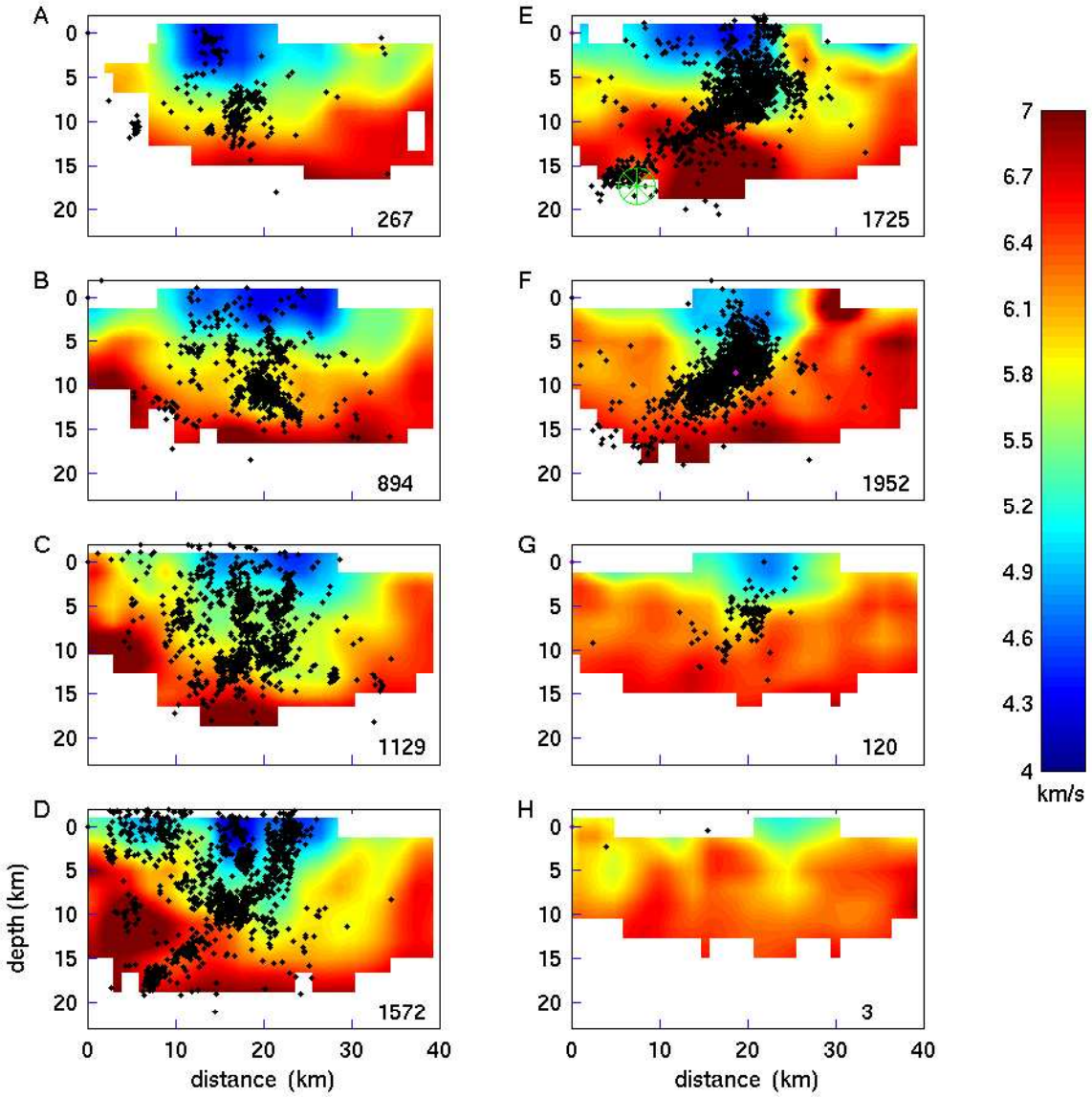

Figure 9: Similar to Fig. 7 but showing events recorded in 1994 only.

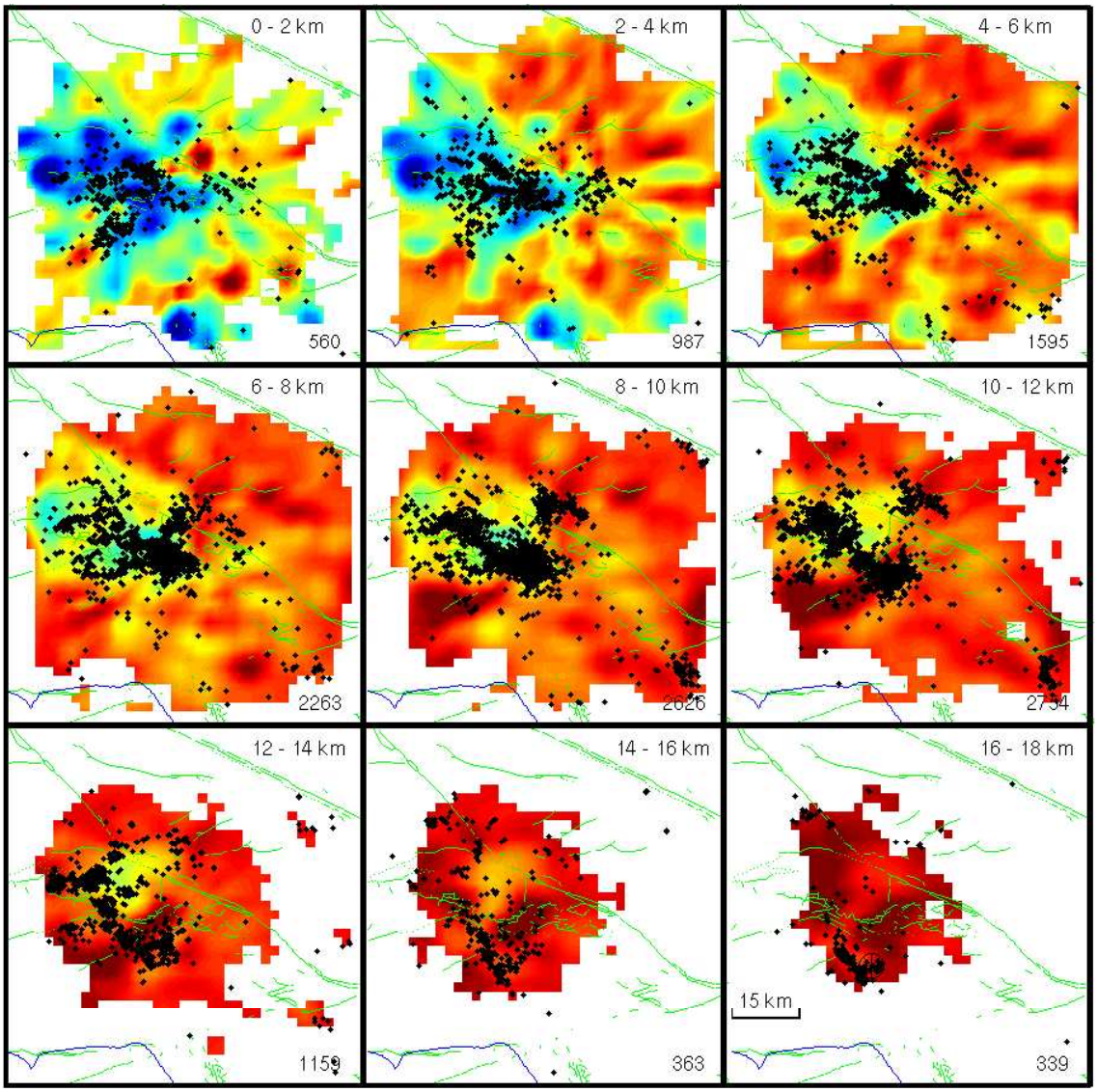

Figure 10: Map view of the velocity model as a function of depth. The numbers on the right upper corners indicate the depth range. Also shown are the inversion locations. The numbers on the right lower corners indicate the number of events. Note below 10 km depth the events that occur within or close to a high velocity wedge.

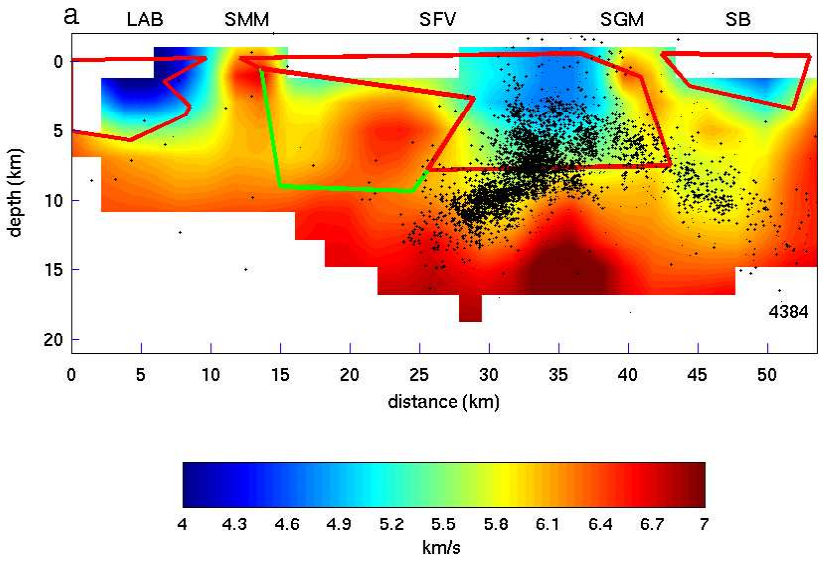

Figure 11: Similar to Fig. 4 for blocks covered by at least five rays. The fact that the initial model is one-dimensional indicates that the velocities in Fig. 4 for the blocks not shown here were determined in earlier iterations. Also shown are the events within box **a** in Fig. 1. The box width is 8 km. Note that the Northridge and San Fernando aftershocks are underlain by a wedge of basement, with the seismicity taking place where velocities are lower. We interpret this result as an indication that this basement wedge remained elevated during the opening of the basin, with the observed seismicity occurring in the weaker sedimentary rocks around its flanks.

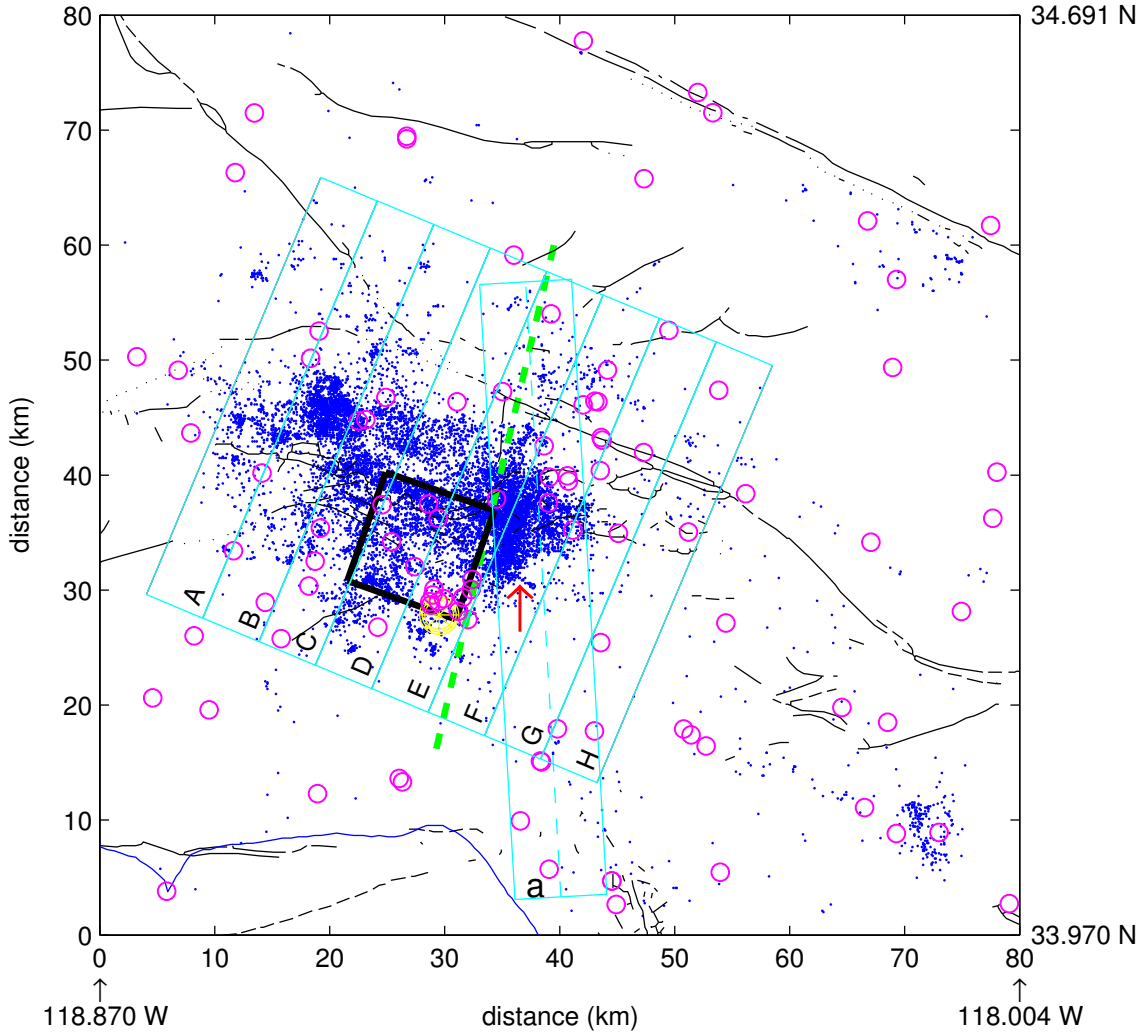

Figure 12: Epicenters of the 1980-2000 events in Fig. 1 as determined by Hauksson et al. (2003). The events are somewhat more scattered than in Fig. 1. The events in the boxes A through H are shown in cross section form in Figure 13.

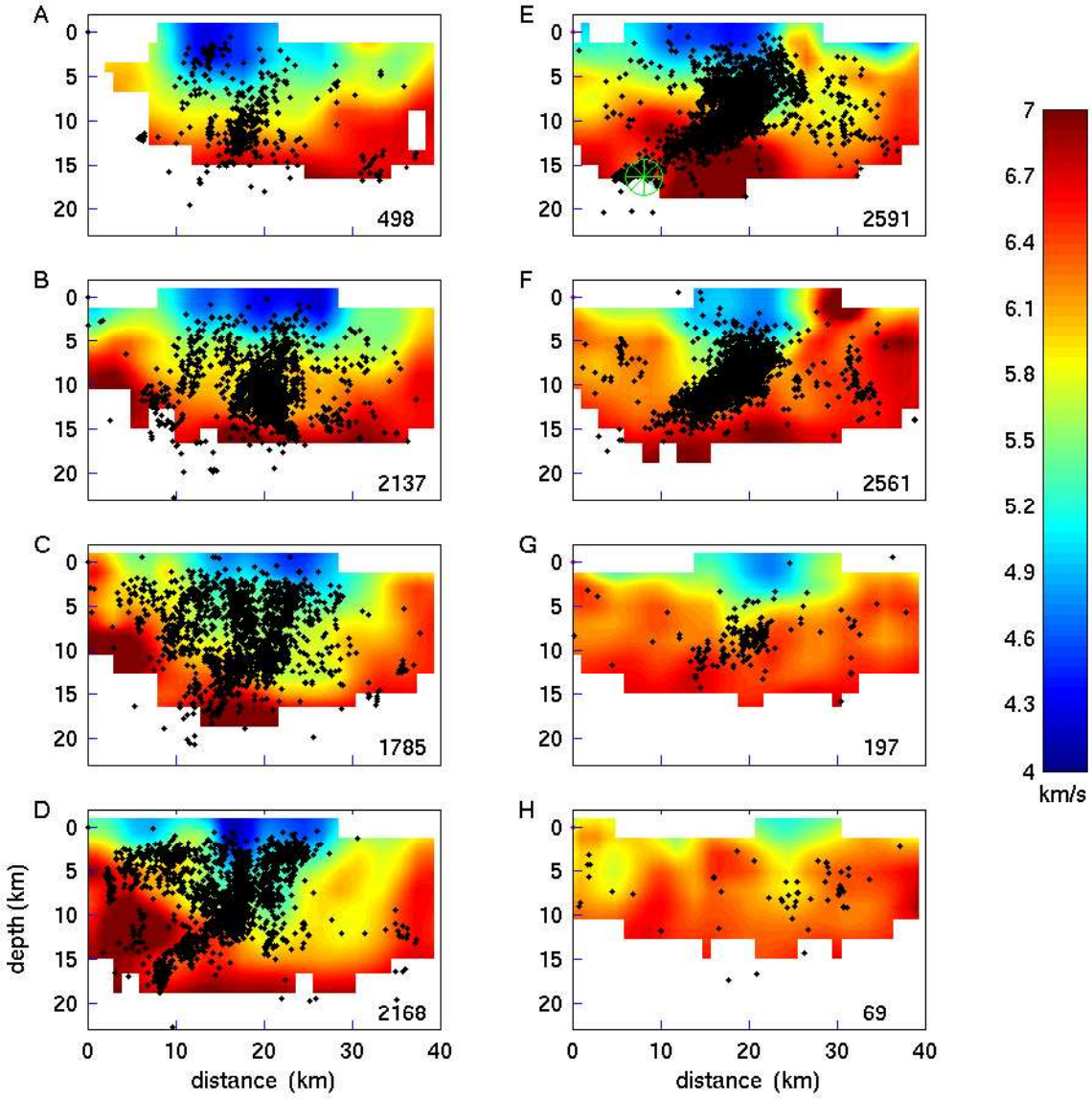

Figure 13: Similar to Fig. 7 for the Hauksson et al. (2003) locations.

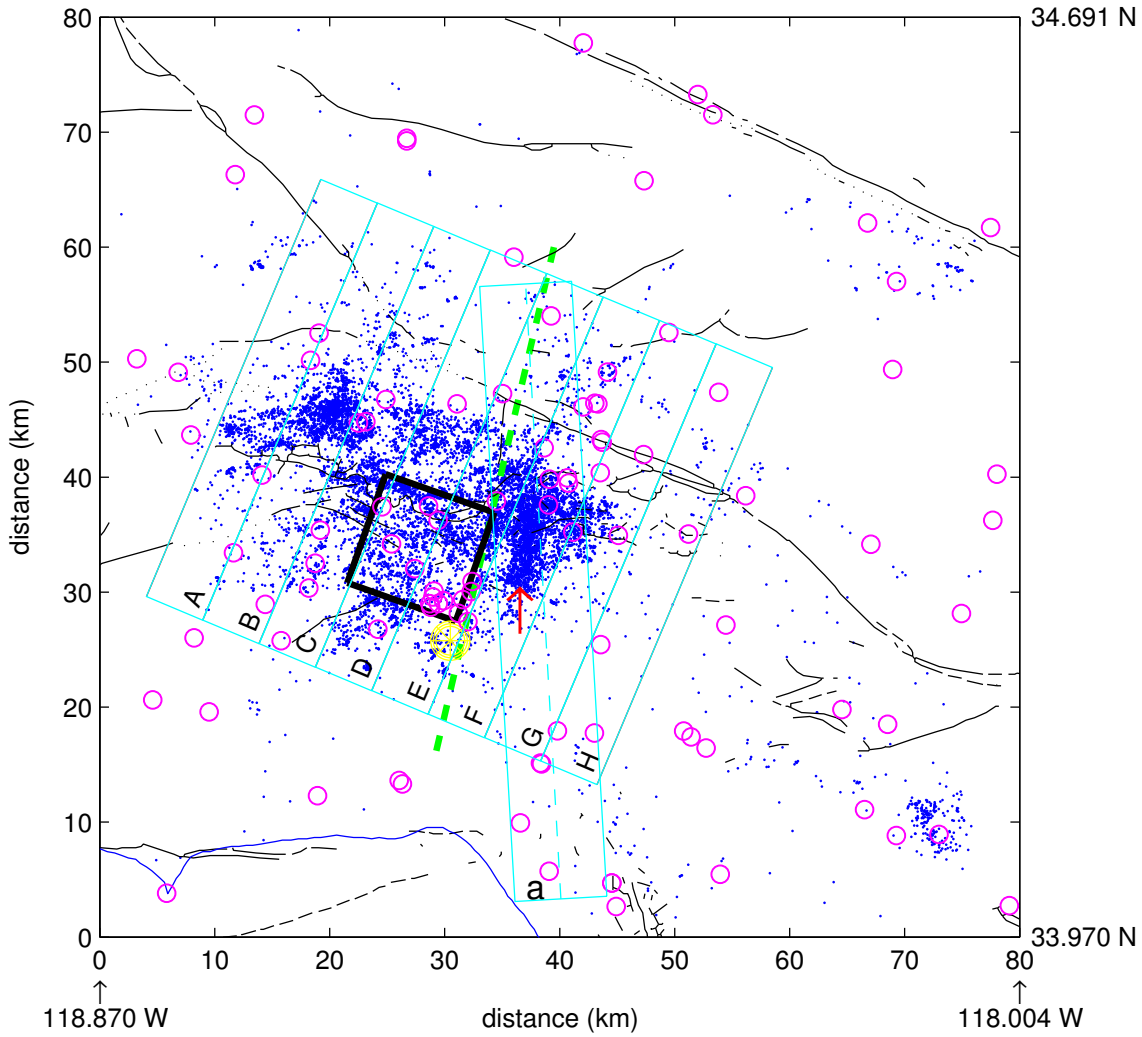

Figure 14: Epicenters of the 1980-2000 events in Fig. 1 as determined by Shearer et al. (2003). The events in the boxes A through H are shown in cross section form in Figure 15.

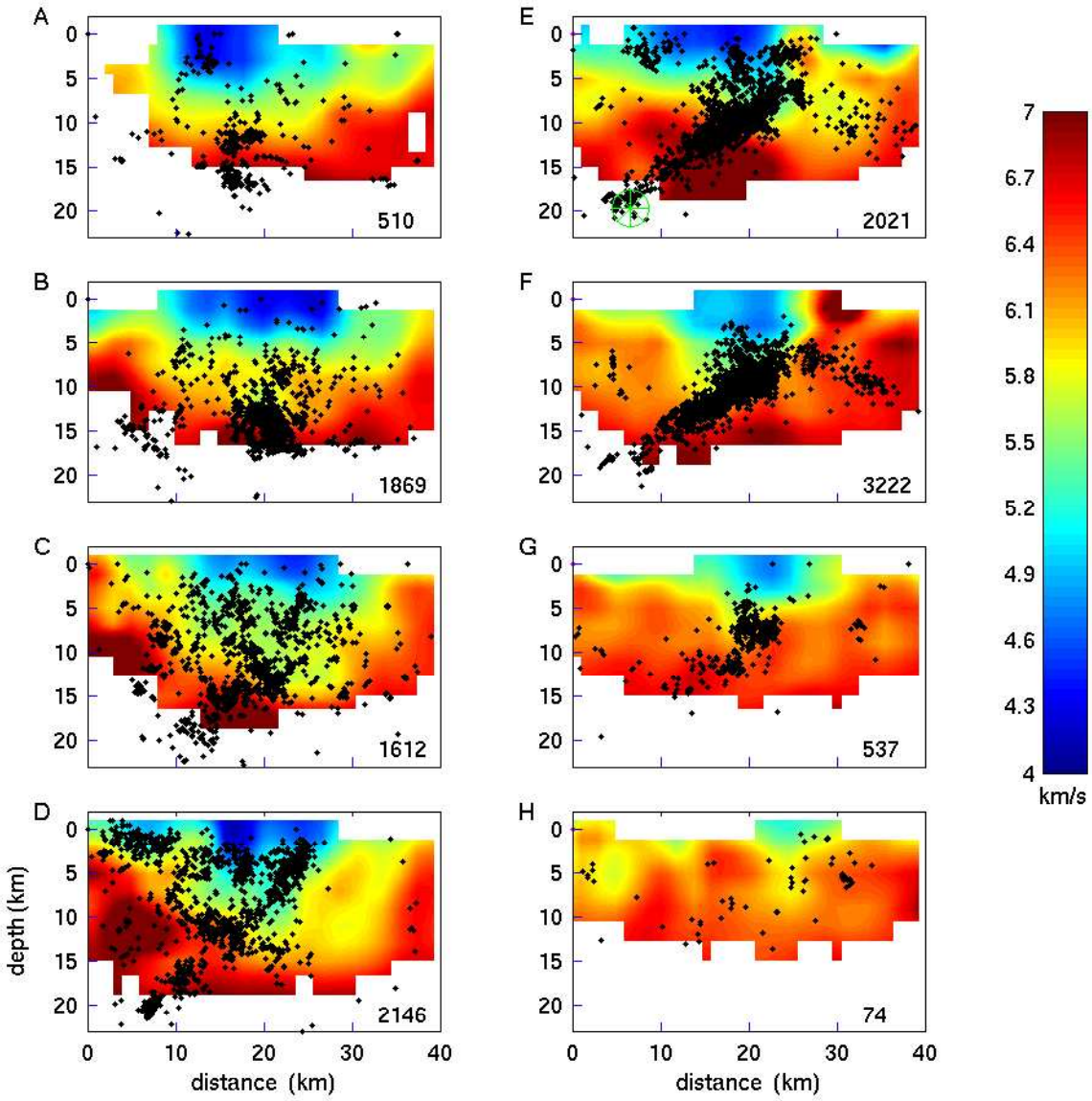

Figure 15: Similar to Fig. 7 for the Shearer et al. (2003) event locations. Note that the events are consistently deeper than in Fig. 7.